Supplementary Materials for

A Deep Learning Approach to Increase the Value of Satellite Data for $PM_{2.5}$ Monitoring in China

Bo Li [1], Cheng Liu [2,3,4,5,*], Qihou Hu [3], Mingzhai Sun [2], Chengxin Zhang [2], Yizhi Zhu [2], Ting Liu [1], Yike Guo [6], Gregory R. Carmichael [7] and Meng Gao [8,9]

Table S1. Number of CNEMC stations at different population densities (people/km^2) and the area percentage of different population densities (within parentheses).

	<1	1~25	25~100	100~500	500~1000	>1000
North China	0(7)	2(18)	0(25)	12(30)	37(16)	125(4)
East China	0(3)	0(0)	1(6)	39(59)	56(25)	247(7)
South China	0(13)	0(0)	5(7)	37(69)	45(7)	150(4)
Sichuan Basin	0(0)	0(25)	7(17)	33(48)	54(8)	51(2)
Shaanxi Province	0(0)	0(7)	0(30)	41(52)	35(9)	101(2)

Table S2. The occurrences of marked cloudy conditions.

	2017	Spring	Summer	Autumn	Winter	Year
MODIS	North China	0.62	0.66	0.60	0.83	0.67
	Eastern China	0.66	0.76	0.71	0.69	0.71
	South China	0.86	0.88	0.79	0.77	0.83
	Sichuan Basin	0.81	0.80	0.84	0.83	0.82
	Shaanxi Province	0.66	0.66	0.68	0.74	0.68

Table S3 The input data shape

Category	Name	shape type	shape
AOD data	Himawari-8 Current	width,length,time	32,32,4
	Himawari-8 Closeness	width,length,time	32,32,10
	Himawari-8 Period	width,length,time	32,32,7
	MODIS	width,length,band×time	32,32,3×7
Meteorology	rh	width,length,time	32,32,9
	temperature	width,length,time	32,32,9
	pressure	width,length,time	32,32,9
	hpbl	width,length,time	32,32,9
	u	width,length,time	32,32,9

	v	width,length,time	32,32,9
	rh	width,length,height	32,32,12
	temperature	width,length,height	32,32,12
	pressure	width,length,height	32,32,12
	hpbl	width,length,height	32,32,1
	u	width,length,height	32,32,12
	v	width,length,height	32,32,12
Geographic information data	POI	width,length,type	64,64,7
	Traffic Network	width,length,type	64,64,9
	DEM	width,length,type	64,64,1
	GDP	width,length,type	64,64,1
	Tpop	width,length,type	64,64,1
	Land Cover Type	width,length,type	32,32,17
	EVI	width,length,type	32,32,1
	NDVI	width,length,type	32,32,1

Table S4. MODIS MCD12C1 Land Cover Type

Class	Description	Class	Description
0	water	9	savannas
1	evergreen needleleaf forest	10	grasslands
2	evergreen broadleaf forest	11	permanent wetlands
3	deciduous needleleaf forest	12	croplands
4	deciduous broadlead forest	13	urban and built-up
5	mixed forests	14	cropland/natural vegetation mosaic
6	closed shrubland	15	snow and ice
7	open shrublands	16	barren or sparsely vegetated
8	woody savannas		

Table S5. Traffic Network classification.

Class	Description	Class	Description
0	primary	5	track
0	primary_link	5	track_grade
1	secondary	6	trunk
1	secondary_link	6	trunk_link
2	tertiary	6	bridleway
2	tertiary_link	7	unknown
3	motorway	7	unclassified
3	motorway_link	8	footway
4	living_street	8	path
4	residential	8	pedestrian
4	steps		
4	service		
4	cycleway		

Table S6. Point of Interest classification.

Class	Description	Class	Description
01	automobile service	03	health care service
01	car sale	03	accommodation service
01	vehicle maintenance and repair	03	serviced apartment
01	Motorcycle service	04	tourist attraction
01	transportation facilities service	05	education and culture service
02	catering service	06	government organization
02	shopping service	06	financial and insurance service
03	life services	06	incorporated business
03	sport and leisure services	07	factory

Table S7.

The α of bivariate test between each parameter and $PM_{2.5}$.(pearsonr p-value)

α	Himawari-8	MOD	MYD	Tempc	Pressure	RH	HPBL	U	V	DEM	GDP	TPOP
PM2.5	0	0	0	0	0	0	0	0	0	0	0.036	0.01

The α of bivariate test between each parameter and $PM_{2.5}$.(Chi-square p-value)

α	Road	POI	Land Cover Type
PM2.5	0.04	0.04	0

The Maximum Information Coefficient between continuous parameters and $PM_{2.5}$

CIM	Himawari-8	MOD	MYD	Tempc	Pressure	Rh	Hpbl	U	V	DEM	GDP	Tpop	NDVI	EVI
PM2.5	0.27	0.51	0.49	0.31	0.34	0.34	0.30	0.24	0.23	0.74	0.51	0.59	0.27	0.29

Table S8. The spatial ranges of study regions.

	top_latitude	bottom_latitude	left_longitude	right_longitude
North China	45°N	35°N	110°E	120°E
East China	36°N	26°N	112°E	122°E
South China	30°N	20°N	108°E	118°E
Sichuan Basin	36°N	26°N	100°E	110°E
Shaanxi Province	40°N	30°N	105°E	115°E

Table S9. Major features of previous related studies.

Study	Model	Resolution	Study Area	Sample Validation			Space Validation			Time Validation		
				R^2	RMSE	Slop	R^2	RMSE	Slop	R^2	RMSE	Slop
(Ma et al.	Two-Stage	0.1° daily	China (2004~2013)	0.7	27.42	0.79	-	-	-	-	-	-

2016)				9									
(Fang et al. 2016)	TSAM	10km daily	China (2013.6~2014.5)	0.80	22.75	0.79	-	-	-	-	-	-
(Wang et al. 2016)	Linear Regression	0.03° night	Atlanta city (2012.8~2012.10)	-	-	-	0.45	4.11	1.00	-	-	-
(Wei et al. 2016)	GWR	3km daily	China(2014)	0.79	18.60	0.83	-	-	-	-	-	-
(Li et al. 2017)	Geoi-DBN	10km daily	China (2015)	0.88	13.03	0.88	0.82	16.42	0.86	-	-	-
(Yu et al. 2017)	Gauss	10km daily	China (2013)	0.81	21.87	0.73	-	-	-	-	-	-
(Xiao et al. 2017)	Multiple Imputation	1km daily (full coverage)	Yangtze River Delta (2013~2014)	0.81	25.00	0.99	-	-	-	-	-	-
(He and Huang 2018)	GTWR	3km daily	China (2015)	0.80	18.00	0.81	0.75	20.73	0.79	0.58	28.24	0.61
(Fu et al. 2018)	Mixed-Effect	0.01° night	Beijing (2013.12~2014.11)	-	-	-	0.86	32.4	-	-	-	-
(Shtein et al. 2019)	GAM	1km daily	Italy (2013~2015)	-	-	-	0.80	6.06	0.99	-	-	-
(Chen et al. 2019)	SMLM	0.05° hourly (daytime)	covers most of China (2016)	0.85	17.30	0.86	-	-	-	-	-	-
(Zhang et al. 2019)	ST-LME	5km hourly (daytime)	east-central China(2015.7~2017.7)	0.80	-	-	-	-	-	-	-	-
(Wei et al. 2019)	ST-RF	1km daily	China (2015)	0.85	15.57	0.82	0.83	16.63	0.81	0.63	24.83	0.62
(Bi et al. 2019)	RF	1km daily (full coverage)	New York State (2015)	0.82	2.16	1.05	-	-	-	-	-	-
(Zhang et al. 2019)	XGBoost	3km daily (nearly full coverage)	China (2014~2015)	0.87	16.33	-	0.86	17.89	-	0.67	25.87	-
(Tang et al. 2019)	Two-Stage RF	1km hourly (full day) (full coverage)	Yangtze River Delta (2017)	-	-	-	0.86	12.4	0.81	-	-	-
(Liu et al. 2019)	RF	5km hourly(daytime)	China(2016)	0.86	17.20	0.81	-	-	-	-	-	-
(Jiang et al. 2020)	Two-Stage RF	1km hourly(full day) (full coverage)	China(2018)	0.85	11.02	-	0.74	14.65	-	-	-	-
(Wei et al. 2020)	Enhanced ST-ET	1km daily	China (2017~2018)	0.89	10.33	0.86	0.88	10.93	0.85	-	-	-
(Park et	CNN-RF	12km daily	America (2011)	0.8	2.55	1.04	0.6	3.55	1.00	0.8	2.55	1.05

al. 2020)				4			9			4		
Xiao et.al (2018)	Model	0.1°daily	China (2013~2017)	0.79	21	1	0.76	22	1	0.73	24	1
Liu et. al (2019)	RF	5km hourly (daytime)	China (2016)	0.86	17.3	0.82	-	-	-	-	-	-
Mhawish et. al (2020)	LME+RF	1km daily	IGP (2018.7~2019.6)	0.87	28	0.84	0.87	28.1	0.84			
Guo et. Al (2021)	RF	1km daily	China (2017)	0.74	16.29	0.61	0.72	16.73	0.6	0.36	20.41	0.34
Schneider et. al (2020)	RF	1km daily	Great Britain (2008~2018)	0.77	4.042	1.05	0.66	2.24	0.99	0.8	3.38	1.06
Dong et. al (2020)	RF-BPNN	0.05°hourly (daytime)	China (2017)	0.8	18.54		0.76	20.27				
This study	ST-NN	0.01° hourly (full day)(full coverage)	covers most of China (2017~2020)	0.88	12.98	0.99	0.85	14.33	1.02	0.86	14.69	1.02

References:

Ma, Z.; Hu, X.; Sayer, A. M.; Levy, R.; Zhang, Q.; Xue, Y.; Tong, S.; Bi, J.; Huang, L.; Liu, Y., Satellite-based spatiotemporal trends in PM2. 5 concentrations: China, 2004–2013. Environmental health perspectives 2016, 124, (2), 184-192.

Fang, X.; Zou, B.; Liu, X.; Sternberg, T.; Zhai, L., Satellite-based ground PM2. 5 estimation using timely structure adaptive modeling. Remote Sensing of Environment 2016, 186, 152-163.

Wang, J.; Aegerter, C.; Xu, X.; Szykman, J. J., Potential application of VIIRS Day/Night Band for monitoring nighttime surface PM2. 5 air quality from space. Atmospheric environment 2016, 124, 55-63.

You, W.; Zang, Z.; Zhang, L.; Li, Y.; Pan, X.; Wang, W., National-scale estimates of ground-level PM2. 5 concentration in China using geographically weighted regression based on 3 km resolution MODIS AOD. Remote Sensing 2016, 8, (3), 184.

Li, T.; Shen, H.; Yuan, Q.; Zhang, X.; Zhang, L., Estimating ground-level PM2. 5 by fusing satellite and station observations: a geo-intelligent deep learning approach. Geophysical Research Letters 2017, 44, (23), 11,985-11,993.

Yu, W.; Liu, Y.; Ma, Z.; Bi, J., Improving satellite-based PM 2.5 estimates in China using Gaussian processes modeling in a Bayesian hierarchical setting. Scientific reports 2017, 7, (1), 1-9.

Xiao, Q.; Wang, Y.; Chang, H. H.; Meng, X.; Geng, G.; Lyapustin, A.; Liu, Y., Full-coverage high-resolution daily PM2. 5 estimation using MAIAC AOD in the Yangtze River Delta of China. Remote Sensing of Environment 2017, 199, 437-446.

He, Q.; Huang, B., Satellite-based mapping of daily high-resolution ground PM2. 5 in China via space-time regression modeling. Remote Sensing of Environment 2018, 206, 72-83.

Fu, D.; Xia, X.; Duan, M.; Zhang, X.; Li, X.; Wang, J.; Liu, J., Mapping nighttime PM2. 5 from VIIRS DNB

using a linear mixed-effect model. Atmospheric Environment 2018, 178, 214-222.
Shtein, A.; Kloog, I.; Schwartz, J.; Silibello, C.; Michelozzi, P.; Gariazzo, C.; Viegi, G.; Forastiere, F.; Karnieli, A.; Just, A. C., Estimating daily PM2. 5 and PM10 over Italy using an ensemble model. Environmental science & technology 2019, 54, (1), 120-128.
Chen, J.; Yin, J.; Zang, L.; Zhang, T.; Zhao, M., Stacking machine learning model for estimating hourly PM2. 5 in China based on Himawari 8 aerosol optical depth data. Science of The Total Environment 2019, 697, 134021.
Zhang, T.; Zang, L.; Wan, Y.; Wang, W.; Zhang, Y., Ground-level PM2. 5 estimation over urban agglomerations in China with high spatiotemporal resolution based on Himawari-8. Science of the total environment 2019, 676, 535-544.
Wei, J.; Huang, W.; Li, Z.; Xue, W.; Peng, Y.; Sun, L.; Cribb, M., Estimating 1-km-resolution PM2. 5 concentrations across China using the space-time random forest approach. Remote Sensing of Environment 2019, 231, 111221.
Bi, J.; Belle, J. H.; Wang, Y.; Lyapustin, A. I.; Wildani, A.; Liu, Y., Impacts of snow and cloud covers on satellite-derived PM2. 5 levels. Remote sensing of environment 2019, 221, 665-674.
Chen, Z.-Y.; Zhang, T.-H.; Zhang, R.; Zhu, Z.-M.; Yang, J.; Chen, P.-Y.; Ou, C.-Q.; Guo, Y., Extreme gradient boosting model to estimate PM2. 5 concentrations with missing-filled satellite data in China. Atmospheric Environment 2019, 202, 180-189.
Tang, D.; Liu, D.; Tang, Y.; Seyler, B. C.; Deng, X.; Zhan, Y., Comparison of GOCI and Himawari-8 aerosol optical depth for deriving full-coverage hourly PM2. 5 across the Yangtze River Delta. Atmospheric Environment 2019, 217, 116973.
Liu, J.; Weng, F.; Li, Z., Satellite-based PM2. 5 estimation directly from reflectance at the top of the atmosphere using a machine learning algorithm. Atmospheric Environment 2019, 208, 113-122.
Jiang, T.; Chen, B.; Nie, Z.; Ren, Z.; Xu, B.; Tang, S., Estimation of hourly full-coverage PM2. 5 concentrations at 1-km resolution in China using a two-stage random forest model. Atmospheric Research 2021, 248, 105146.
Wei, J.; Li, Z.; Cribb, M.; Huang, W.; Xue, W.; Sun, L.; Guo, J.; Peng, Y.; Li, J.; Lyapustin, A., Improved 1 km resolution PM 2.5 estimates across China using enhanced space–time extremely randomized trees. Atmospheric Chemistry and Physics 2020, 20, (6), 3273-3289.
Park, Y.; Kwon, B.; Heo, J.; Hu, X.; Liu, Y.; Moon, T., Estimating PM2. 5 concentration of the conterminous United States via interpretable convolutional neural networks. Environmental Pollution 2020, 256, 113395.
Xiao, Q., Chang, H. H., Geng, G., and Liu, Y.: An Ensemble Machine-Learning Model To Predict Historical PM2.5 Concentrations in China from Satellite Data, Environmental Science & Technology, 52, 13260-13269, 10.1021/acs.est.8b02917, 2018.
Liu, J.; Weng, F.; Li, Z. Satellite-based PM2.5 estimation directly from reflectance at the top of the atmosphere using a machine learning algorithm. Atmospheric Environment 2019, 208, 113-122, doi:https://doi.org/10.1016/j.atmosenv.2019.04.002.
Mhawish, A., Banerjee, T., Sorek-Hamer, M., Bilal, M., Lyapustin, A. I., Chatfield, R., and Broday, D. M.: Estimation of High-Resolution PM2.5 over the Indo-Gangetic Plain by Fusion of Satellite Data, Meteorology, and Land Use Variables, Environmental Science & Technology, 54, 7891-7900, 10.1021/acs.est.0c01769, 2020.
Guo, B., Zhang, D., Pei, L., Su, Y., Wang, X., Bian, Y., Zhang, D., Yao, W., Zhou, Z., and Guo, L.: Estimating PM2.5 concentrations via random forest method using satellite, auxiliary, and ground-level station dataset at multiple temporal scales across China in 2017, Science of The Total Environment, 778, 146288, https://doi.org/10.1016/j.scitotenv.2021.146288, 2021.
Schneider, R., Vicedo-Cabrera, A. M., Sera, F., Masselot, P., Stafoggia, M., de Hoogh, K., Kloog, I., Reis, S., Vieno, M., and Gasparrini, A.: A Satellite-Based Spatio-Temporal Machine Learning Model to Reconstruct Daily PM2.5 Concentrations across Great Britain, Remote Sensing, 12, 3803, 2020.

Dong, L., Li, S., Yang, J., Shi, W., and Zhang, L.: Investigating the performance of satellite-based models in estimating the surface PM2.5 over China, Chemosphere, 256, 127051, https://doi.org/10.1016/j.chemosphere.2020.127051, 2020.

Table S10. The influences of different data quality treatments on the performance of the model.

train	test	RMSE	MAE	Slope	R-square
without empty data	without empty data	16.53	10.10	0.98	0.87
	without outlier data	14.62	9.55	0.96	0.87
without outlier data	without empty data	18.24	10.46	1.06	0.84
	without outlier data	14.30	9.46	1.00	0.87

Table S11. Data quality control status.

	2017(N)		2018(N)		2019(N)		2020(N)		Rate
	outlier	not null	outlier	not null	outlier	not null	outlier	not null	
North China	188547	1340252	186265	1241169	180120	1257882	175359	1228487	0.14
East China	420792	2663647	364102	2525520	395344	2478030	381681	2503516	0.15
South China	325190	1957469	280304	1875939	298656	1865894	342722	1908516	0.16
Sichuan Basin	170788	1132051	168210	1043238	167905	1044349	170819	1062847	0.16
Shaanxi Province	189610	1369405	184997	1280065	184698	1277902	199430	1301866	0.15

Table S12. Statistics of number of stations used for training and testing

	All Number(N)	Training Number(N)	Testing Number(N)	All Sample Number(N)			
				2017	2018	2019	2020
North China	176	150	26	1340252	1241169	1257882	1228487
East China	343	308	35	2663647	2525520	2478030	2503516
South China	237	213	24	1957469	1875939	1865894	1908516
Sichuan Basin	145	130	15	1132051	1043238	1044349	1062847
Shaanxi Province	177	159	18	1369405	1280065	1277902	1301866

Table S13. Validation results for different scales of spatial region mask.

Train	36°~44°N	27°~35°N						
Area	111°~119°E	123°~121°E						
Mask	38.2°~40.2°N	29°~33°N	30°~33°N	31°~33°N	32°~33°N	32°~33°N	31°~32°N	31°~32°N
Area	114.1°~116.1°E	116°~120°E	117°~120°E	118°~120°E	118°~119°E	119°~120°E	118°~119°E	119°~120°E
R-squ	Num Rate	Nu Rate	Num Rate	Num Rate	Num Rate	Num Rate	Num Rate	Num Rate

are	ber	(%)	mbe r	(%)	ber	(%)	ber	(%)	ber	(%)	ber	(%)	ber	(%)	ber	(%)
<0.5	/	/	5	0.05	1	0.01	/	/	/	/	/	/	/	/	/	/
0.5~0.6	/	/	9	0.09	4	0.05	/	/	/	/	/	/	/	/	/	/
0.6~0.65	/	/	14	0.14	6	0.08	/	/	/	/	/	/	/	/	/	/
0.65~0.7	/	/	34	0.35	21	0.28	2	0.05	/	/	/	/	/	/	/	/
0.7~0.75	1	0.17	24	0.24	24	0.32	9	0.22	/	/	1	0.12	/	/	2	0.18
0.75~0.8	5	0.83	6	0.06	10	0.13	19	0.48	3	0.25	6	0.76	/	/	5	0.45
>0.8	/	/	6	0.06	10	0.13	10	0.25	9	0.75	1	0.12	9	1	4	0.37

Table S14. Hourly validation of Near Real Time model (trained with data from 2017 to 2020 and test with 2020).

R-square	Number	CNEMC mean	ST-NN mean
<0.4	10	16.26	19.81
0.4~0.45	8	35.28	30.51
0.45~0.5	21	35.73	35.44
0.5~0.55	26	41.17	43.72
0.55~0.6	30	40.70	43.96
0.6~0.65	20	39.47	41.74
0.65~0.7	26	41.26	45.04
>0.7	9	42.30	47.40

Table S15. Assess the ability of the model to capture different levels of contamination through accuracy and precision.

	North China NRT model (>75μg/m³)		29°~33°N,116°~120°E mask (>75μg/m³)		30°~33°N,117°~120°E mask (>75μg/m³)		31°~33°N,118°~120°E mask (>75μg/m³)	
value	Number		Number		Number		Number	
	accuracy	precision	accuracy	precision	accuracy	precision	accuracy	precision
<0.4	/	14	/	9	/	0	/	1
0.4~0.5	/	6	/	16	/	1	/	0
0.5~0.6	/	15	/	21	/	6	/	4
0.6~0.7	/	28	/	28	/	13	/	13
0.7~0.8	/	28	/	14	/	24	/	11
0.8~0.9	31	22	3	7	/	20	/	8
>0.9	100	18	95	3	82	18	45	8

Table S16. Validation results under different training and test proportions

test:train	1:9	2:8	3:7	4:6	5:5	6:4	7:3
R-squre	0.81	0.81	0.78	0.77	0.76	0.76	0.74
RMSE(μg/m³)	16.15	16.6	17.57	17.87	18.67	18.55	19.32

Table S17. Percentage of data in different regions exceeding 250 μgm^{-3}

Region	North China	East China	South China	Sichuan Basin	Shaanxi Province
Rate (%)	0.76	0.18	0.02	0.12	0.65

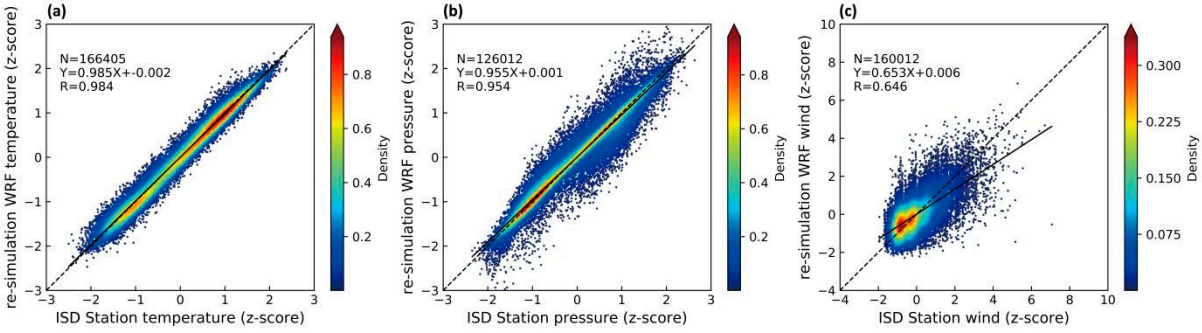

Figure S1. Validation of meteorological parameters simulated by WRF with observation data at ISD (Integrated Surface Database) stations. (a) temperature. (b) pressure. (c) wind speeds.

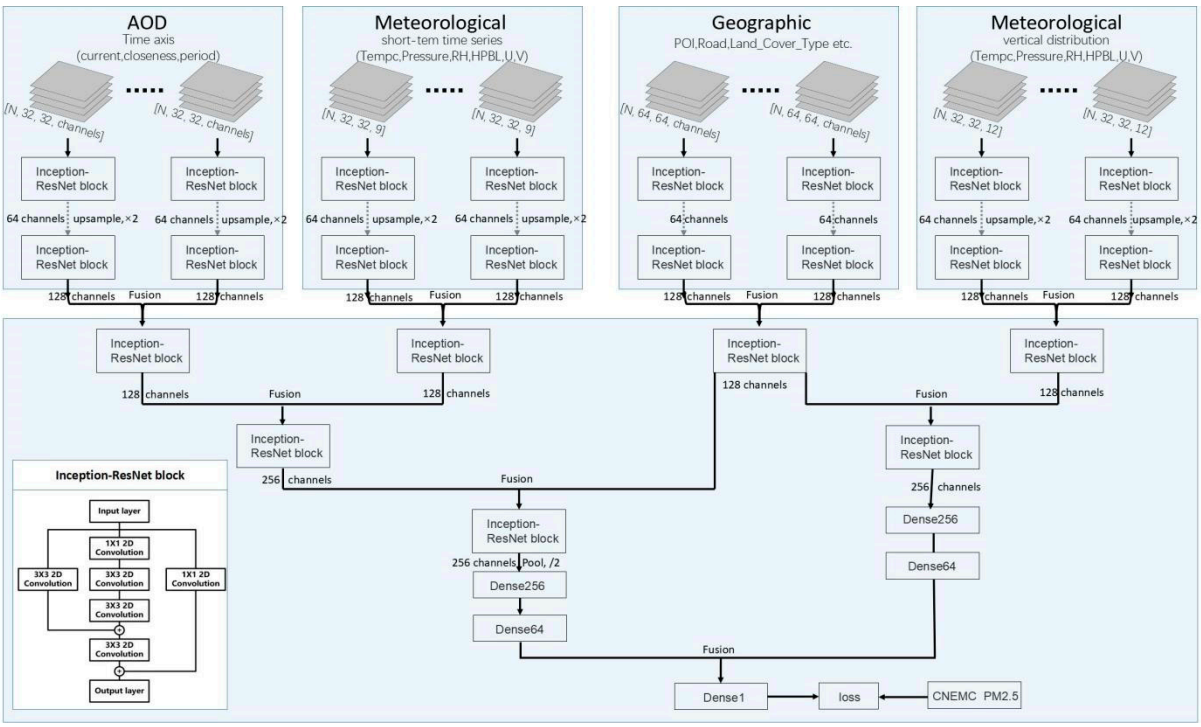

Figure S2. The architecture of the ST-NN model. Inputs data include AOD, meteorological data and geographic data. All the input variables have the 4-D dimensions as [N, lat_size, lon_size, channel]. N means the batch size, lat_size and lon_size means the scale of the data at latitude and longitude, channels represent the types or the height/time dimension of the data. Considering the computational efficiency and the generalization ability of the model, we choose N as 4. First, feature extraction was used for individual data by Inception-ResNet, which is an efficient feature extraction process. After it, we up-sampled the data at 0.05°×0.05°resolution using the transposed convolution layer, which is a learning-based up-sampling method. We used the strides as 2 and a 2×2 convolution kernel to double size of the input data. Accordingly, all data had the same size. Then we mined the characteristics of each variable and fused the data with same types by concatenate layer. Then the temporal and spatial features were extracted by fusing the time-series of aerosol and meteorological data with the geographic information data. The final result was obtained through the fully

connected layer.

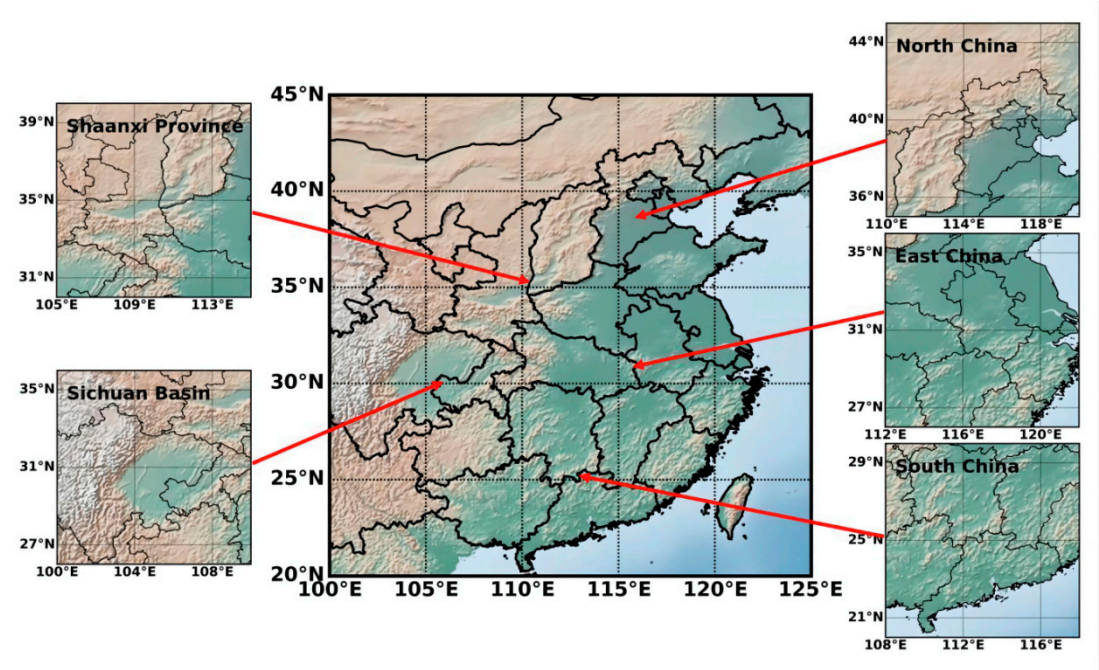

Figure S3. Locations and spatial range of major study regions. Study regions include North China, East China, South China, Sichuan Basin and Shaanxi Province.

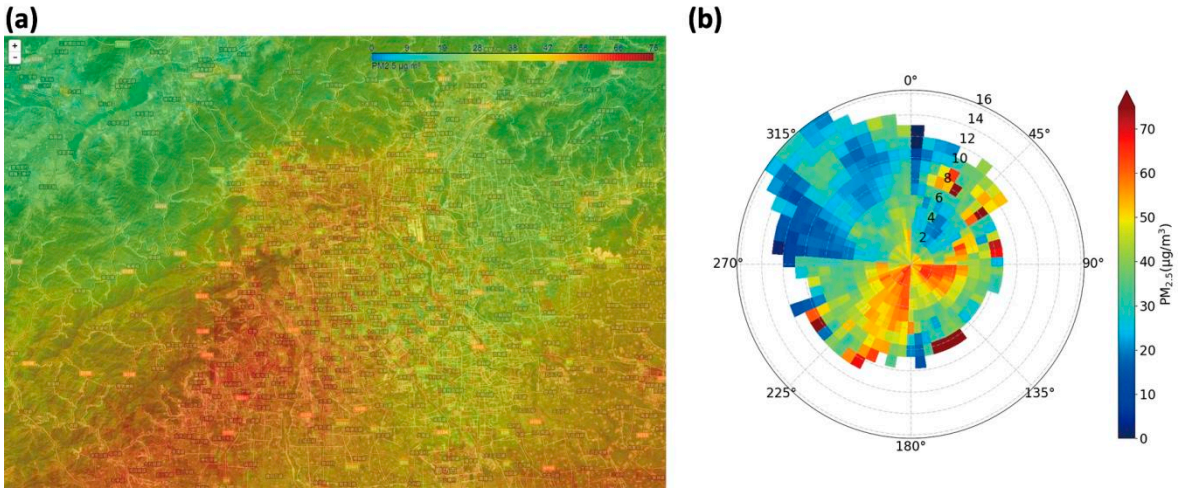

Figure S4. The annual average distribution of $PM_{2.5}$ in Beijing (a). b is a rose, with radius representing wind speed and the color indicating mean $PM_{2.5}$ concentrations. 0° is due north and 90° is due east. It can be seen that the main pollution comes from the southwest, significantly influenced by topography and transmission.

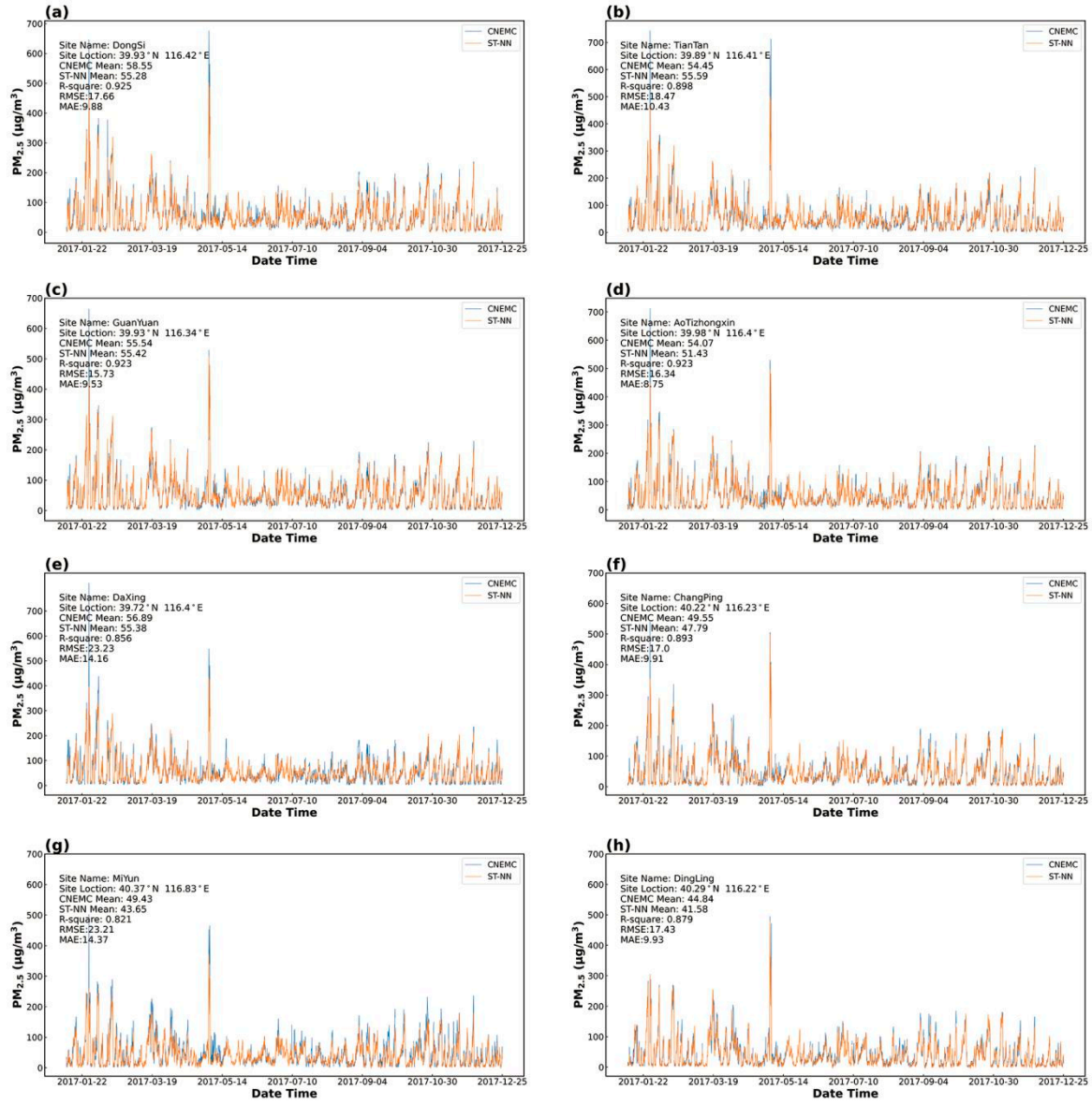

Figure S5. ST-NN model predicted and ground-level observed (not used in training) time series of $PM_{2.5}$ in Beijing stations. (a) Dongsi station in Beijing. (a) Tiantan station in Beijing. (c) Guanyuan station in Beijing. (d) Aotizhognxin station in Beijing. (e) Daxing station in Beijing. (f) Changping station in Beijing. (g) Miyun station in Beijing. (h) Dingling station in Beijing. (a-d) stations are in city, and (e-h) are rural stations.

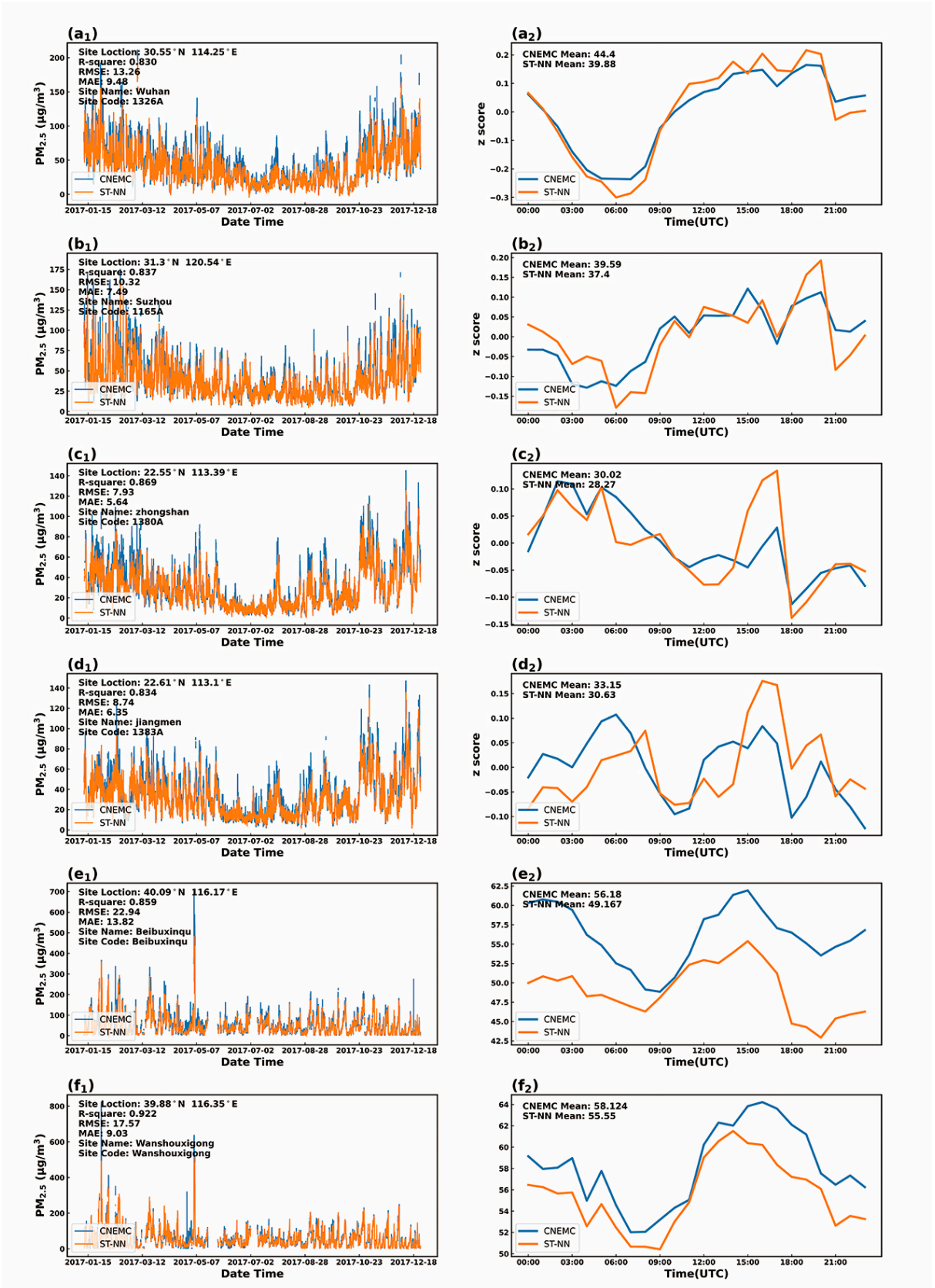

Figure S6. ST-NN model predicted and ground-level observed (not used in training) time series (2017) of $PM_{2.5}$ in China, and comparisons of their diurnal features. Left column: ST-NN model predicted and observed time series of $PM_{2.5}$ in Wuhan (a_1), Suzhou (b_1),

Zhongshan (c_1), Jiangmen (d_1), Guanyuan in Beijing (e_1), Miyun in Beijing (f_1); Right column: ST-NN model predicted and observed diurnal variation of $PM_{2.5}$ in Wuhan (a_2), Suzhou (b_2), Zhongshan (c_2), Jiangmen (d_2), Beibuxinqu in Beijing (e_2), Wanshouxigong in Beijing (f_2). Its vertical axis is the z-score coordinate. $z-\text{score}=\frac{X-\mu}{\sigma}$, μ is the sample mean and σ is the sample standard deviation.

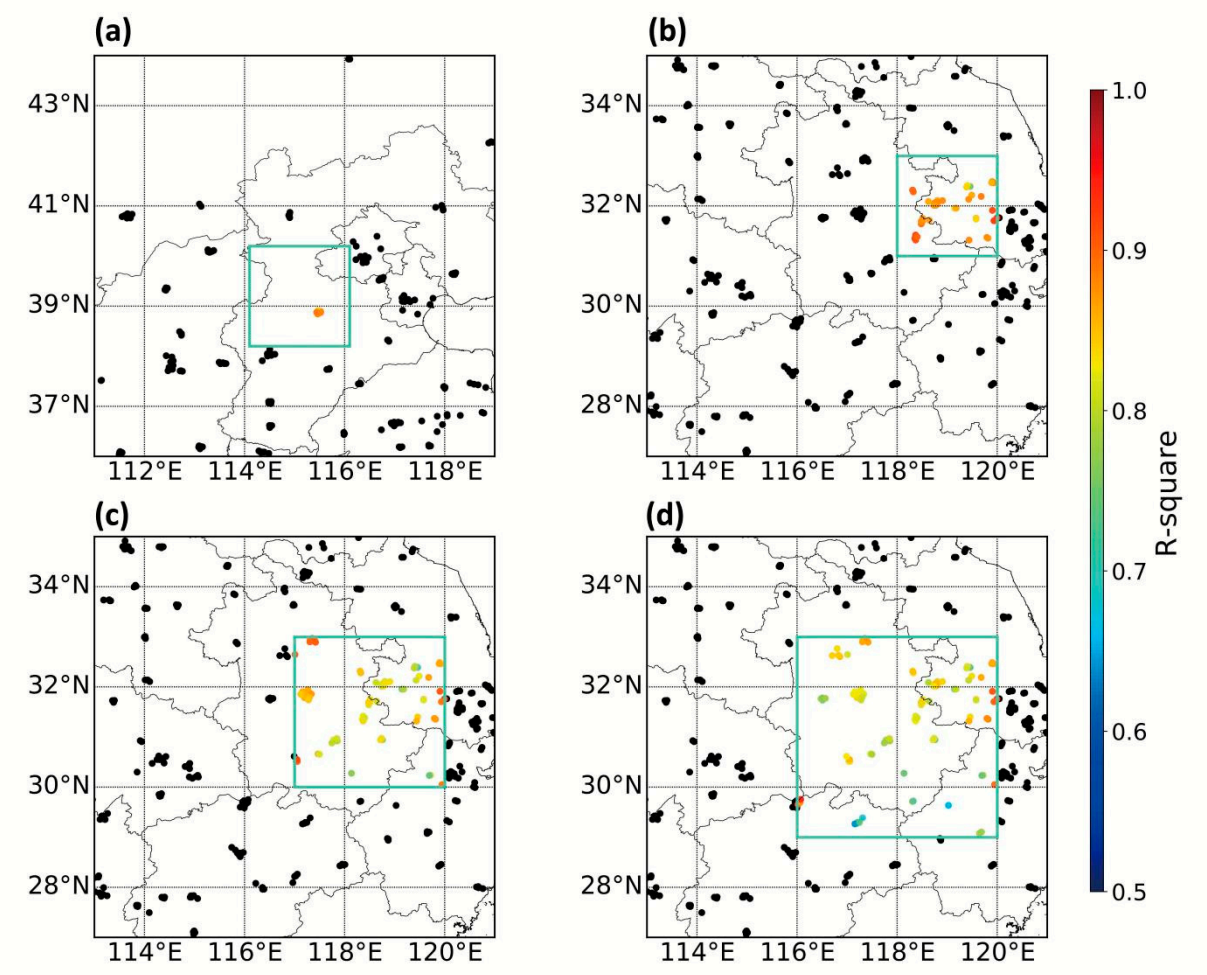

Figure S7. The block distribution of the regional mask validation. Validation was carried out for different spatial mask scales, the black points are the training sites, and the R-square distribution of the validation sites is enclosed by the solid blue line.

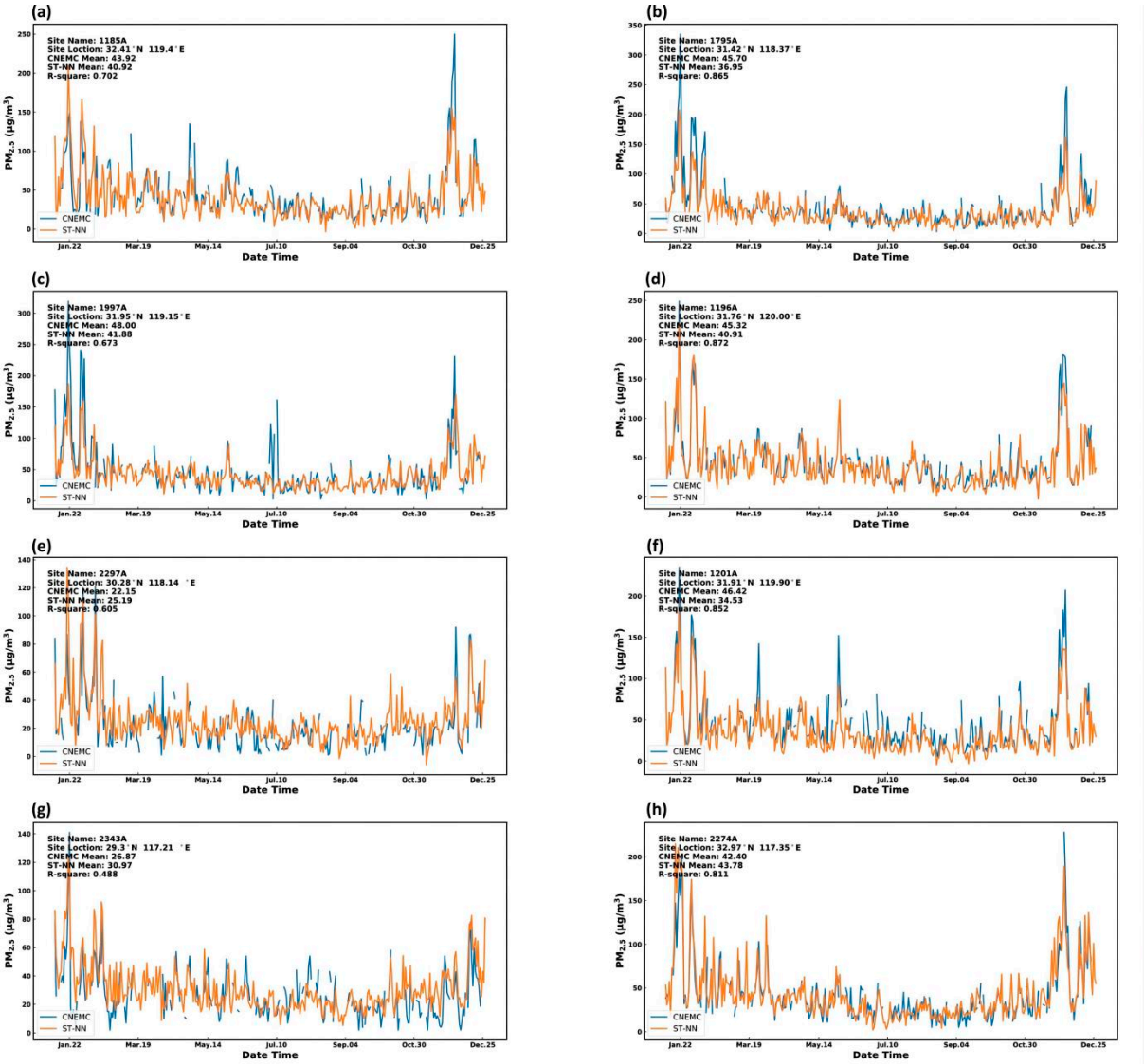

Figure S8. Time series of the regional mask performed (FigureS6b,c,d). (a,b) are the 1◦x1◦ mask validation in the East China. (c,d) are the results of 2◦x2◦ mask validation in the East China. (e,f) are the validation of 3◦x3◦ mask in East China. (g,h) are the validation of 4◦x4◦ mask in East China. And (a,b,c,g) are urban stations. (d,e,f,h) are rural stations.

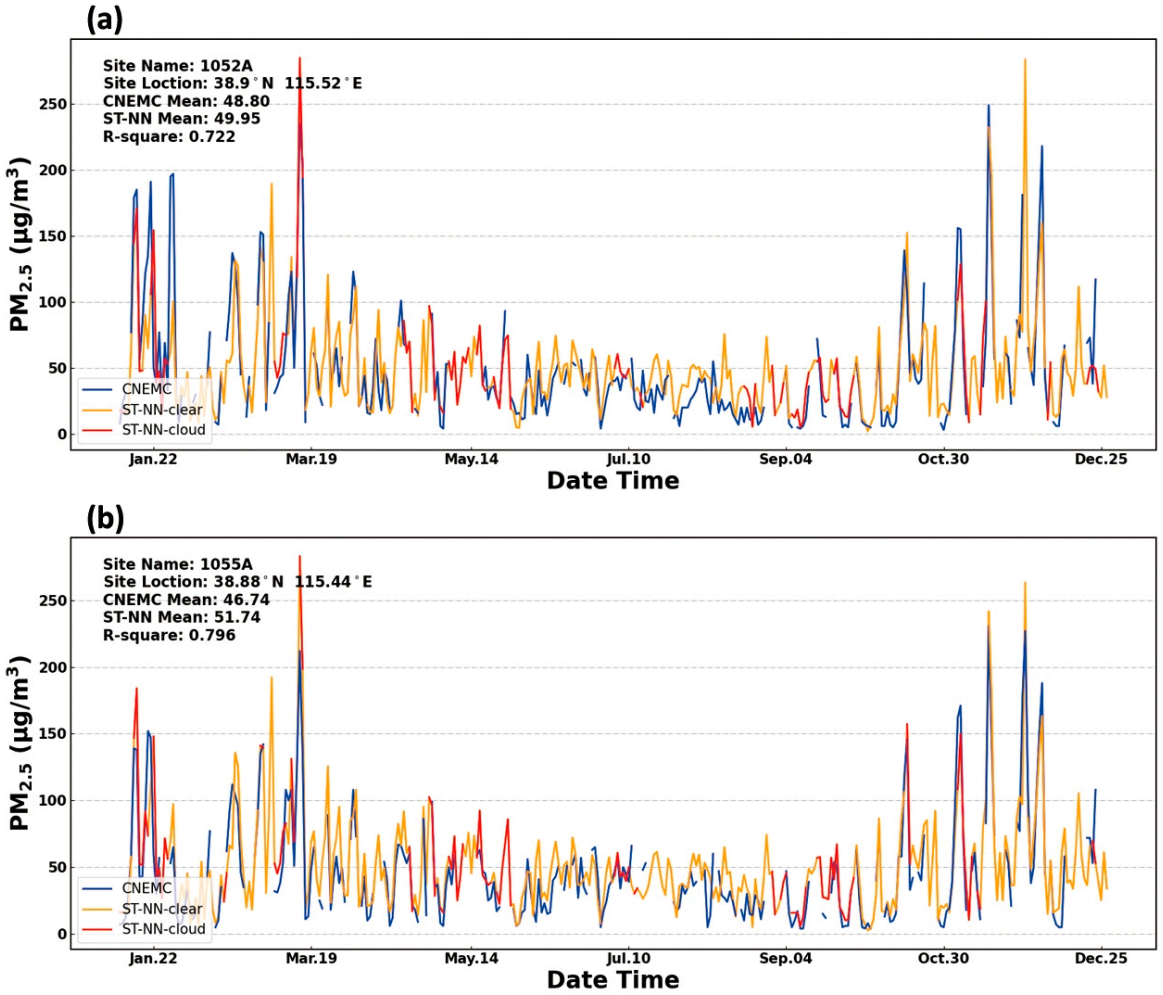

Figure S9. Time series of the regional mask performed (FigureS6a), they are the 2◦x2◦ mask validation in the North China. The blue line is the CNEMC data, the orange line is the ST-NN result for clear day, the red line is the ST-NN result for cloudy day. a is a rural station, b is an urban station.

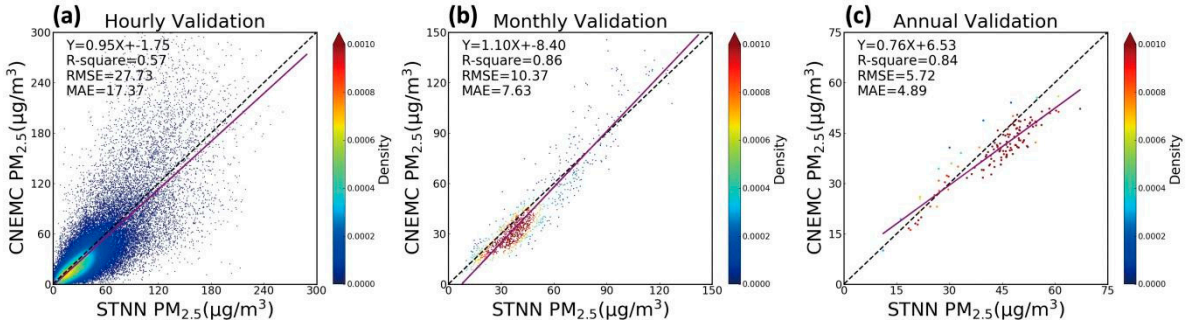

Figure S10. Density scatterplots of the ST-NN model (trained with data from 2017 to

2020 and test with 2020) with hourly(a),monthly(b),annual(c) validation. The fitting line is in purple, and the 1:1 standard line is the black dotted line.

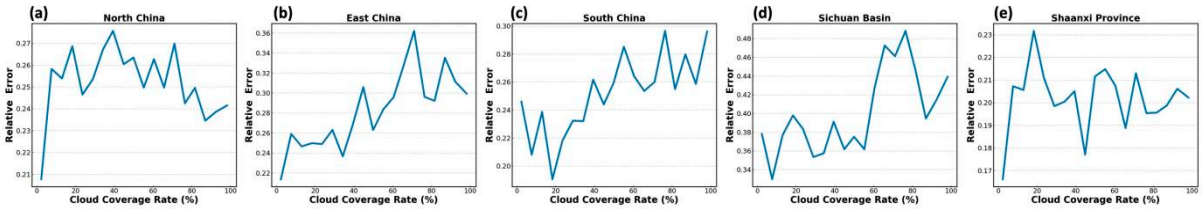

Figure S11. Relative error of cross validation under different cloud coverage rates.

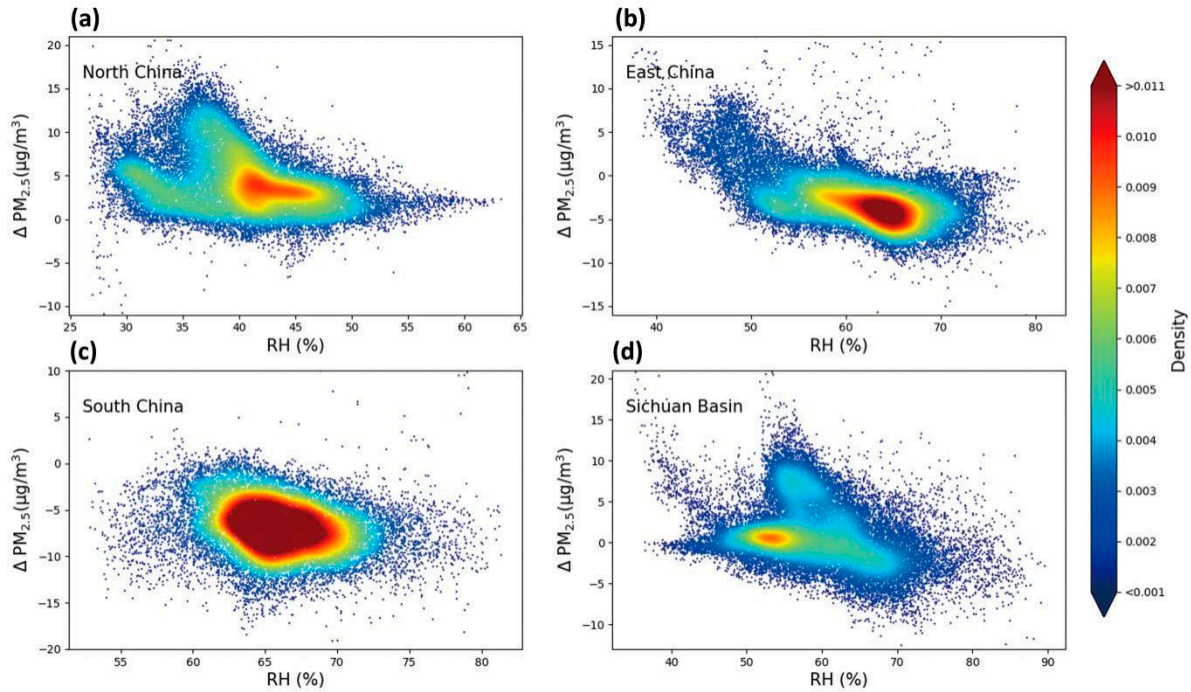

Figure S12. The density distribution diagram of changes in predicted $PM_{2.5}$ concentrations as a function of relative humidity in marked cloudy conditions. (a) North China. (b) East China. (c) South China. (d) Sichuan Basin.

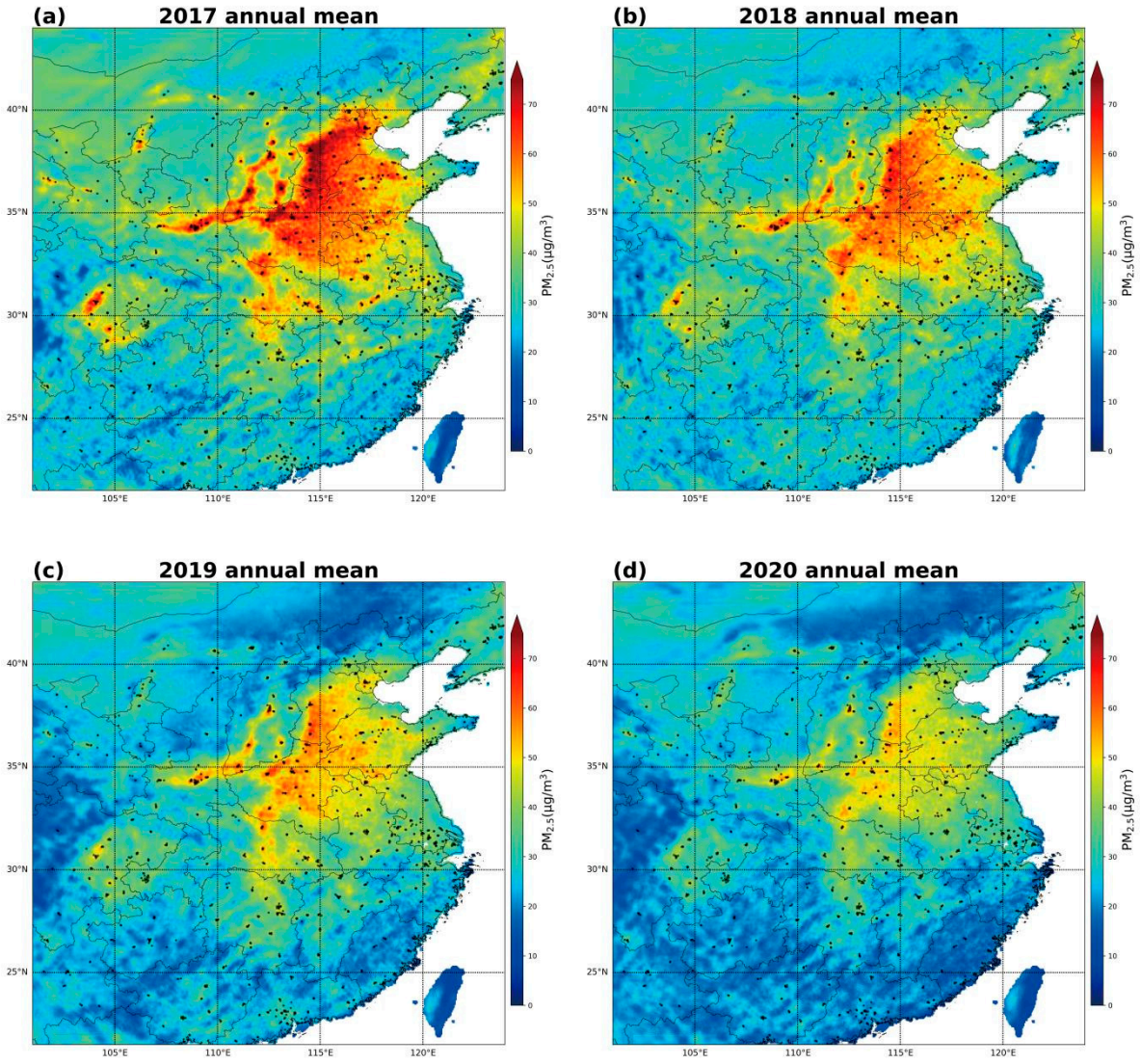

Figure S13. The distribution of predicted annual mean concentrations of $PM_{2.5}$ and the locations of monitoring sites.

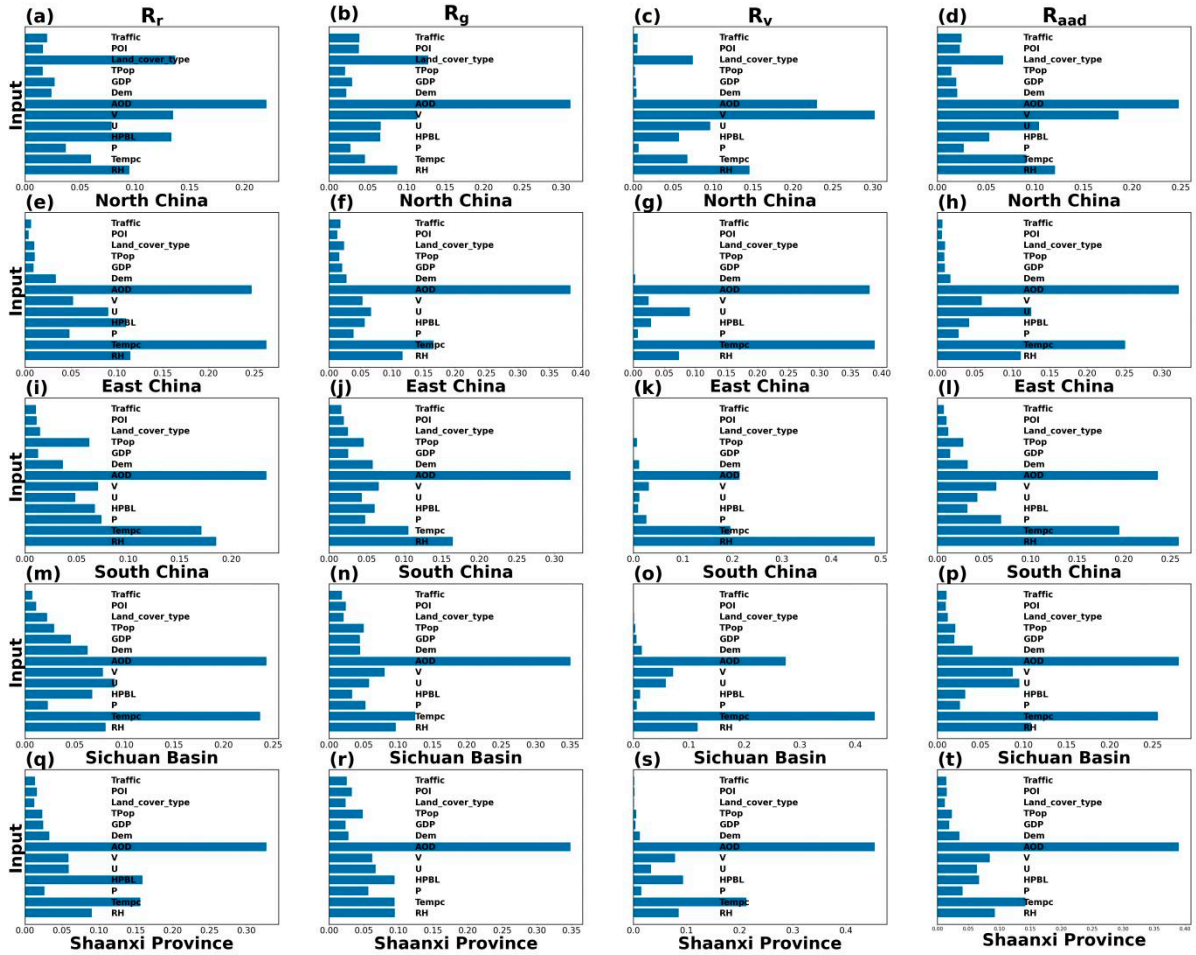

Figure S14. Relative importance indicators (R_r: Relative range; R_g: Relative gradient; R_v: Relative variance; R_{AAD}: Relative average absolute deviation) of input variables for different regions. (a-d) North China. (e-h) East China. (i-l) South China. (m-p) Sichuan Basin. (q-t) Shaanxi Province.

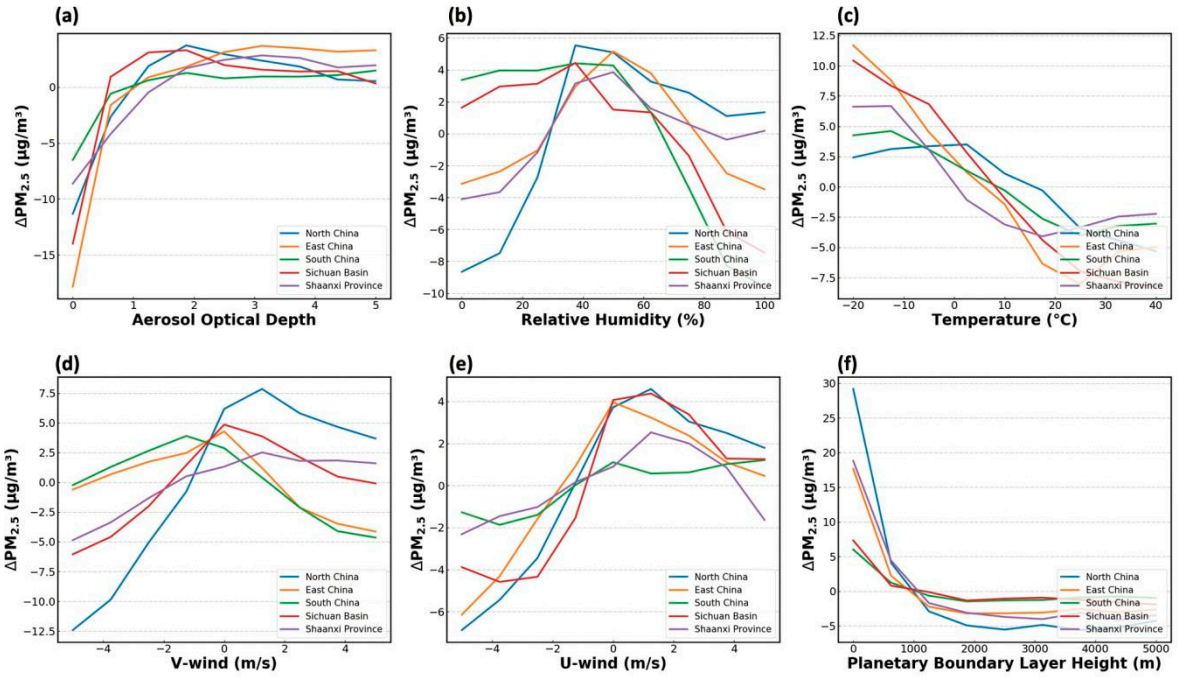

Figure S15. Results of sensitivity analysis of key variables. The influence of relative humidity is mainly due to the hygroscopic growth of $PM_{2.5}$ and the wet removal which is more pronounced in North China. The effect of temperature is mainly seasonal. Low boundary layer pressure leads to higher surface $PM_{2.5}$ concentrations.

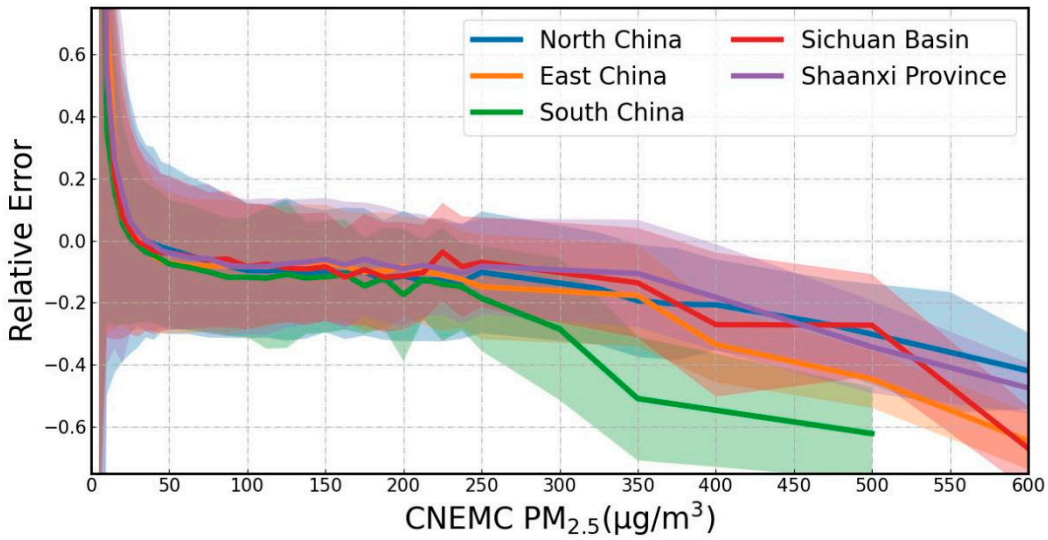

Figure S16. Relative error varies with $PM_{2.5}$ concentrations in different regions. Five lines with different colors represent errors for North China, East China, South China, Sichuan

Basin, and Shaanxi Province.

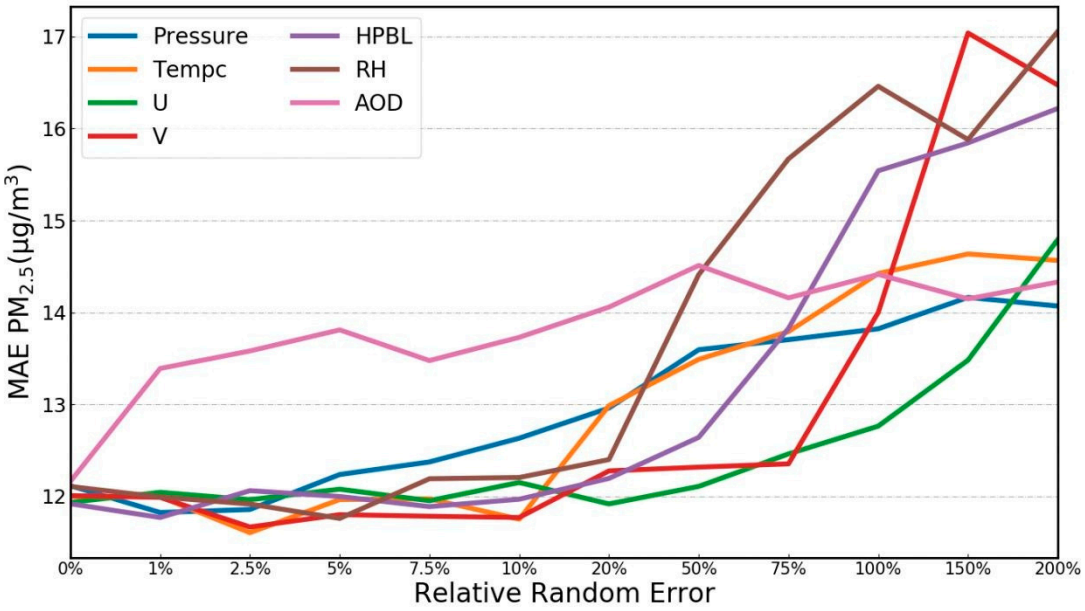

Figure S17. The relationship between the mean absolute error of the model and the relative error of different input data. Seven lines with different colors represent model inputs: pressure, temperature, zonal wind (U), meridional wind (V), boundary layer height, relative humidity, and AOD.

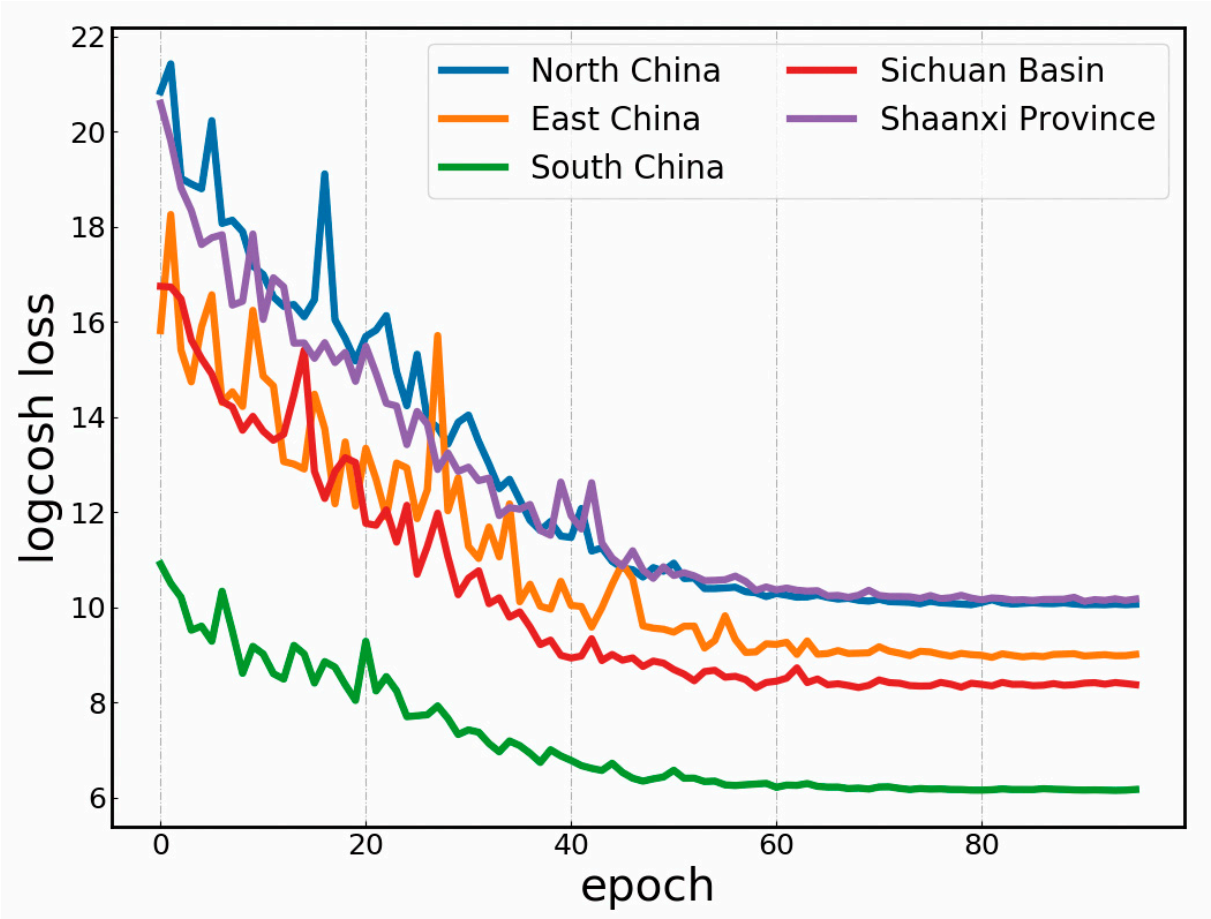

Figure S18. The performance of the validation data logcosh loss function for models built for different regions. Five lines with different colors represent results for North China, East China, South China, Sichuan Basin, and Shaanxi Province.

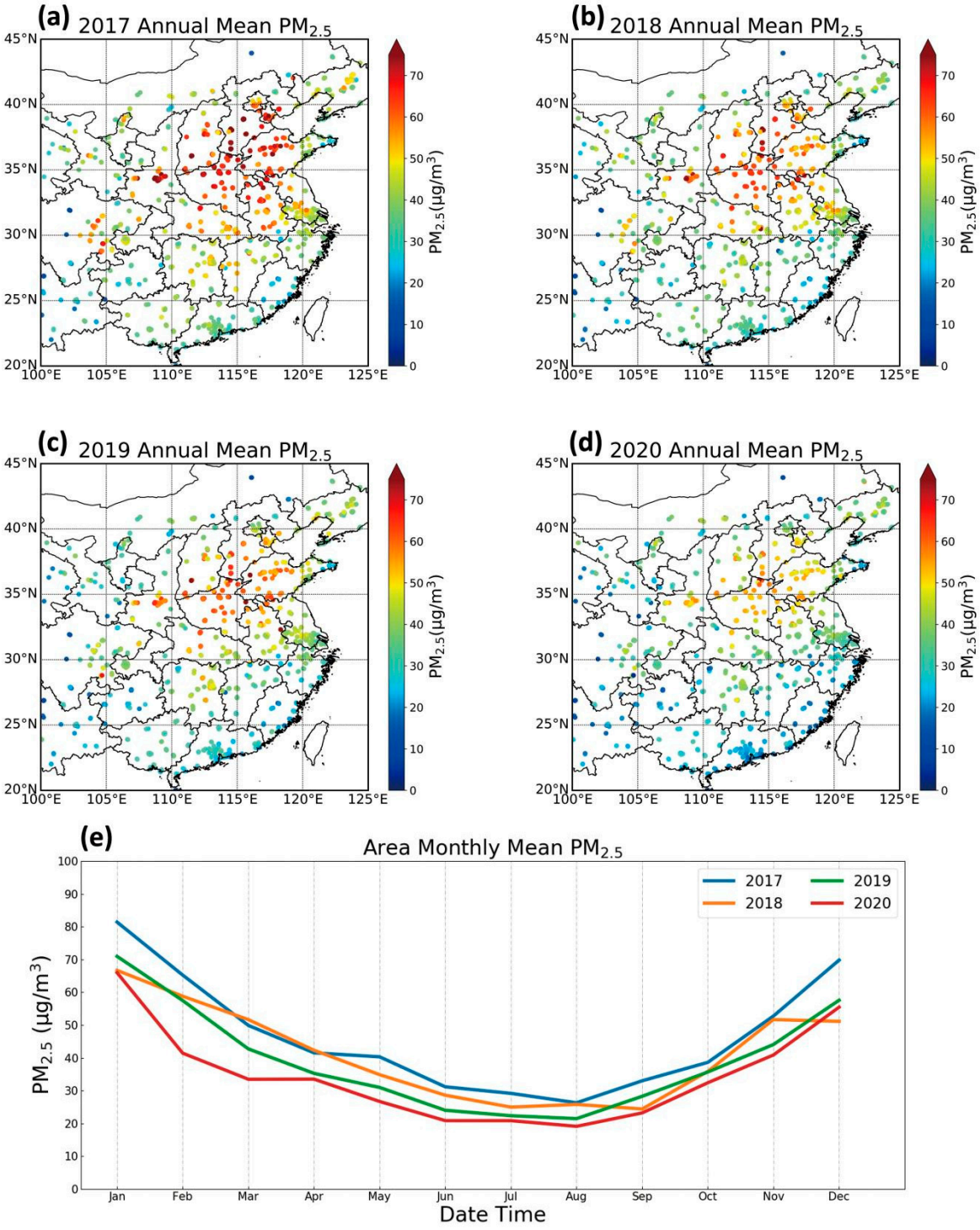

Figure S19. The spatiotemporal distribution of CNEMC observed $PM_{2.5}$ concentrations. (a) Year 2017. (b) Year 2018. (c) Year 2019. (d) Year 2020. (e) Monthly variations.